Cellulose (2023) 30:289–301
https://doi.org/10.1007/s10570-022-04895-x

ORIGINAL RESEARCH

A green attapulgite bacterial cellulose imprinted aerogel for selective adsorption and recovery of Dy(III)

Xudong Zheng · Tongtong Xu · Wen Sun · Jinfeng Mei · Man Zhou · Zhongyu Li

Received: 9 May 2022 / Accepted: 10 October 2022 / Published online: 21 October 2022

Abstract Recycling dysprosium (Dy) from an environment can not only alleviate the industrial crisis, but also reduce the ecological pollution caused by Dy(III). The cost of the materials used to adsorb rare earth ions is generally high, which is not conducive to the wide application of adsorbents in the rare earth industry. Herein, we developed an inexpensive adsorbent based on a three-dimensional network structure consisting of carboxylated bacterial cellulose, attapulgite, and gelatin to replace high-priced adsorbents. A low-cost and green I-APT-GT-OBC aerogel was prepared by a simple freeze-drying process. To test the adsorption properties of the composite aerogel, we carried out a series of adsorption experiments. The results showed that the saturated adsorption capacity of Dy(III) by the imprinted aerogel was 48.762 mg g^{-1} when the pH value was 5.0, and the adsorption process was spontaneous, endothermic and entropy increasing. In the competitive adsorption experiment, the K_d value of I-APT-GT-OBC for Dy(III) was 4084.40 mL g^{-1}, which was much higher than that of other aerogels, showing excellent selective adsorption. In conclusion, I-APT-GT-OBC is expected to be a low-cost adsorbent that can efficiently adsorb Dy(III) in water.

Keywords Bacterial cellulose · Attapulgite · Aerogel · Ion imprinting technology · Dysprosium

Supplementary Information The online version contains supplementary material available at https://doi.org/10.1007/s10570-022-04895-x.

X. Zheng (✉) · T. Xu · W. Sun · J. Mei · M. Zhou · Z. Li
School of Environmental and Safety Engineering, Changzhou University, Mingxing Building, Science and Education City, Wujin District, Changzhou 213164, Jiangsu, People's Republic of China
e-mail: zhengks@outlook.com

Z. Li
Jiangsu Key Laboratory of Advanced Catalytic Materials and Technology, School of Petrochemical Engineering, Changzhou University, Changzhou 213164, People's Republic of China

Z. Li
Advanced Catalysis and Green Manufacturing Collaborative Innovation Center, Changzhou University, Changzhou 213164, People's Republic of China

Introduction

Dysprosium (Dy) is a moderately scarce element and is widely used in NdFeB permanent magnets (Padhan et al. 2017; Yadav et al. 2018) and has an irreplaceable role in this industry. In recent years, China has severely restricted the export of rare earths, which has further exacerbated the shortage of Dy minerals (Zheng et al. 2019). In addition, long-term exposure of the environment to Dy will cause damage to the water, soil and ecology, and may also affect human health (Briao et al. 2021). Therefore, in order to meet the dual needs of economy and ecology, humans began to recycle Dy from discarded permanent

magnets. Among various methods for recovering Dy, many scholars have turned their attention to adsorption methods with high efficiency and simple operation. Devi (Devi and Mishra 2019) used cationic surfactant-treated olive bark powder as a bio-sorbent to adsorb Dy(III) in aqueous solutions. It was found that the chemically modified bark powder was superior to the untreated bark powder, and the adsorption efficiency of the treated bark was increased by about 90%. Kaneko (Kaneko et al. 2018) used surfactants to prepare functionalized MPS materials with different pore sizes for the adsorption of Dy(III), and finally determined an MPS material with a pore size of 22 nm. However, there are not many reports of Dy(III) isolating highly selectively from the mixed solution, and ion imprinting technology can prepare specific sites (Fu et al. 2015; Zheng et al. 2022a, b), so ion imprinting technology is expected to achieve this purpose.

In recent years, bacterial cellulose (BC) has become a promising green biomass raw material due to its excellent mechanical properties and biocompatibility (Oshima et al. 2008; Sakwises et al. 2017). More importantly, the 3D network structure of BC has a good pore structure, which can provide a good basis for the adsorption behavior (Doineau et al. 2020). At the same time, a plenty of oxygen-containing groups on the surface of BC, especially hydroxyl groups, provide the possibility for subsequent modification of the material, and carboxylation modification can increase bonding strength between BC and metal ions, thereby achieving efficient adsorption of Dy(III). At present, BC has been widely used in various industries, and many new BC based functional materials have been developed, such as BC films (Xu et al. 2020), BC emulsions (Kedzior et al. 2021), and BC aerogels (Yan et al. 2022). Among them, aerogel with continuous 3D pores process high porosity and large specific surface area, and is the lightest as a solid material (Long et al. 2018; Salimian et al. 2018). Aerogel is a promising adsorption material, and BC can be directly formed into aerogel by conventional drying or freeze-drying. BC aerogel has high mechanical stability and biocompatibility, and it is a good material for adsorbing Dy(III) in water, but there are still problems such as the poor adsorption effect and the lack of adsorption selectivity (Hoshina et al. 2020; Zhang et al. 2021). Therefore, it is significant to modify BC aerogel to improve the adsorption effect of the material. Ion imprinting takes target metal ions as templates and binds to the functional groups of the precursor by complexation or coordination. The template ions were then filtered out of the material with chemical reagents, and the retention of specific recognition holes showed memory effects on the shape, size and coordination geometry of the target metal ions, so as to achieve selective adsorption of rare earth ions (Monier and Abdel-Latif 2013; Hu et al. 2021). Therefore, ion imprinting technology can effectively solve the problem of interfering ion coexistence.

At present, there are many modified substances that can improve the adsorption effect of adsorbents, such as graphene oxide (Ashour et al. 2017; Li et al. 2021), carbon nanotubes (Pegier et al. 2019; Alguacil et al. 2020) and so on, but these materials are generally expensive, and the prepared adsorbents are not cost-effective. Therefore, our current goal is to modify BC aerogel with low-cost raw materials to reduce the preparation cost while maintaining the high adsorption capacity of Dy(III) (Liao et al. 2018). Attapulgite (APT) has a unique layer-chain structure and appears as a rod-like crystal, which has a strong adsorption capacity for metal ions (Liao et al. 2018; Lin et al. 2021; Shang et al. 2021). At present, the proven mineral reserves of APT in the world are about 1.4 billion tons, which is a natural biopolymer that only second to cellulose. Therefore, APT is inherently cheap and non-toxic (Lin et al. 2021). Gelatin (GT) is a macromolecular hydrophilic colloid, and adding GT can greatly improve the mechanical properties of the material (Moradi et al. 2020; Marciano et al. 2021). In addition, GT can be made from raw materials such as fish skin, chicken skin, fish scales and so on. The raw materials are sufficient and cheap, which meets our need to reduce the cost of adsorbents. In summary, our goal is to use BC as the basic structure, introduce APT and GT, and combine with the ion imprinting technology to prepare low-cost imprinted aerogel (I-APT-GT-OBC) with high selectivity and high adsorption capacity for Dy(III).

Experimental section

We prepared a low-cost green I-APT-GT-OBC aerogel, as shown in Fig. 1. The specific steps are as follows.

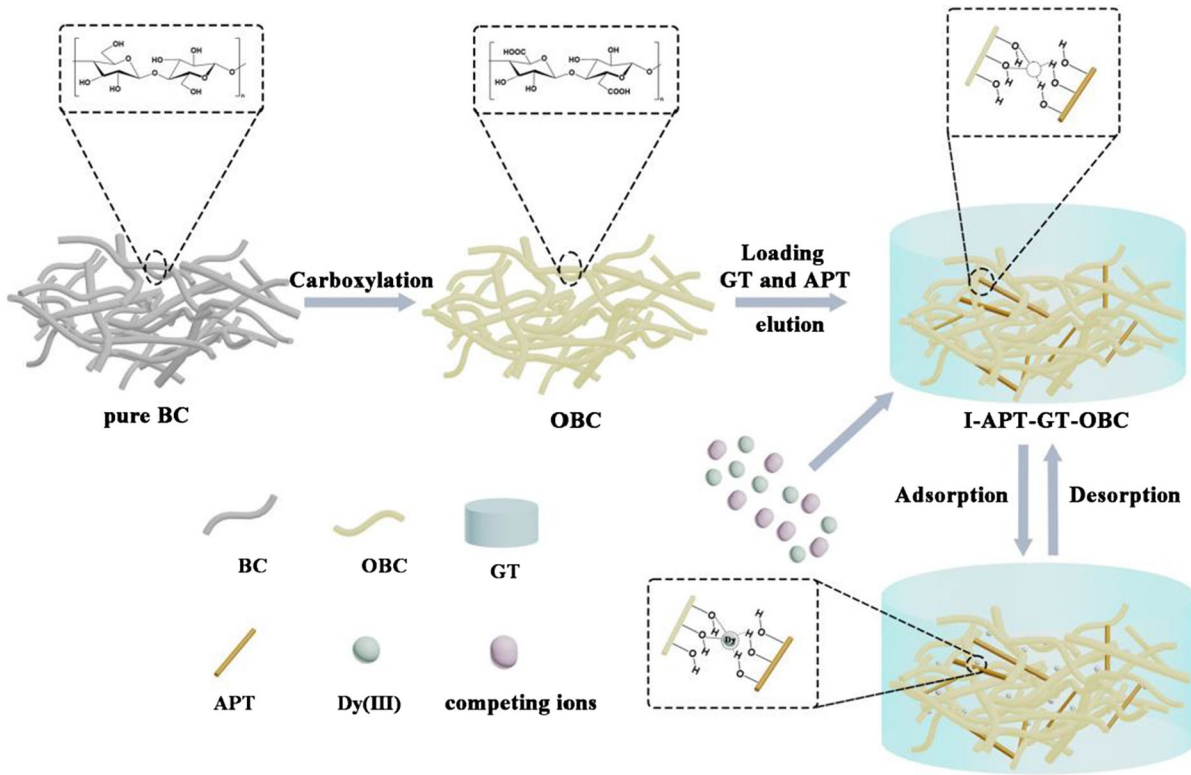

Fig. 1 Synthesis of imprinted I-APT-GT-OBC aerogel

The synthesis of the BC aerogel

The BC aerogel was prepared after ultrasonic treatment of the BC hydrogel for 30 min and freeze-drying for 24 h.

The synthesis of TEMPO-oxidized BC aerogel (OBC)

1.13 g of $NaClO_2$ and 0.016 g of TEMPO were put into a flask containing 90 mL of sodium phosphate buffer solution (0.1 M, pH = 6.8) and mixed well. 16 g of BC wet gel was immersed in the above mixed solution, the flask was shaken at 40 °C for 30 min, and 1 mL of NaClO was added, and the bottle was immediately stoppered, and the flask was shaken at 40 °C for 5 h. Then we added 5 mL of C_2H_5OH to stop the reaction and shaken at room temperature for 30 min. Then we washed the oxidized BC with deionized water. Finally, we immersed the oxidized BC in 0.05 M NaOH solution and shook for 1 h, and we washed the oxidized BC with deionized water until the washing solution was neutral. The prepared OBC can be immersed in deionized water for storage before use. Finally, the OBC wet gel was freeze-dried to prepare aerogel.

The synthesis of APT-GT-OBC aerogel

5 g of OBC hydrogel was immersed in 100 mL of a mixed solution of NaOH/urea/H_2O with a ratio of 7:12:81 and stirred rapidly at − 12 °C. Then we heated 0.2 g of gelatin and poured it into the mixture, added 0.5 g of acidified and purified APT, and sonicated for 30 min. The mixture was freeze-thawed three times, with a freeze–thaw cycle of 12 h at − 20 °C and 4 h of room temperature thawing. After freezing and thawing, the complex was repeatedly washed by distillation until the NaOH and urea were removed and the washing solution was neutral. Finally, freeze-drying was performed to prepare the APT-GT-OBC aerogel.

The synthesis of imprinted APT-GT-OBC aerogel (I-APT-GT-OBC aerogel)

In the above mixture of OBC hydrogel, gelatin and APT, we added 5 mg of $Dy(NO_3)_3$ and adjusted the pH value of the solution to 5.0, then we sonicated for 30 min and freezeed–thawed three times and freezed–dried to prepare the aerogel. The aerogel was transferred to the eluent with a volume ratio of glacial acetic acid to water of 1:9 and soaked for 48 h to remove the template. Finally, the imprinted I-APT-GT-OBC aerogel was prepared by repeated washing with distilled water to remove the residual glacial acetic acid.

In parallel, the materials and equipment involved in the preparation of the experiment, as well as the characterization and adsorption experiments, are described in the supplementary materials.

Results and discussion

Aerogel characterization

SEM

As shown in Fig. 2, the internal microscopic morphologies of the four aerogels were captured by scanning electron microscopy (SEM). Figure 2a showed that the pure BC aerogel has amazing 3D filamentous fibers, and many pores are formed between the fibers. These pores could provide a certain guarantee for the mechanical properties of the composite aerogel, and they also provide a good basis for adsorbing Dy(III) in water. Compared with the pure BC aerogel, the fibers of the OBC aerogel in Fig. 2b were slightly broken, but the original fiber network was basically maintained. The microscopic morphologies

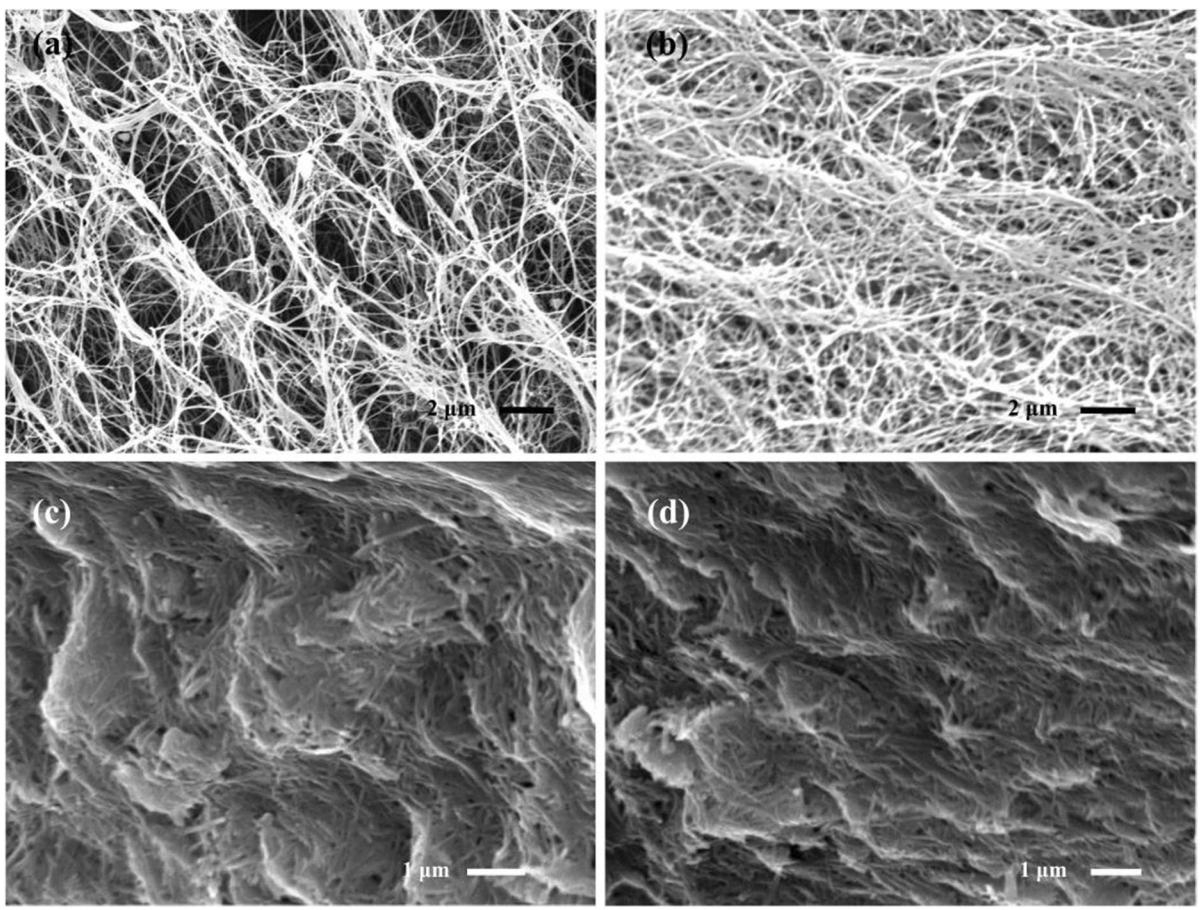

Fig. 2 SEM images of BC (**a**), OBC (**b**), APT-GT-OBC (**c**) and I- APT-GT-OBC (**d**)

of APT-GT-OBC aerogel and I-APT-GT-OBC aerogel were shown in Fig. 2c, d, and it could be seen that there were a large number of slender rod APT adhered to OBC and formed many tiny pores. Compared with the non-imprinted aerogel, the APT on the surface of the eluted imprinted aerogel was more uniform, but the structure did not change significantly, indicating the strong stability of the BC based aerogel.

BET

In order to study the pore structure of the aerogels, the N_2 adsorption–desorption experiments were carried out on four aerogels. The adsorption–desorption isotherms and pore performance of the aerogels were shown in Fig. 3 and Table 1. It could be seen that the S_{BET} of the pure BC aerogel was 37.12 $cm^2\ g^{-1}$. The pore diameter was enlarged, which was due to the partial fracture of the BC fibers caused by carboxylation process, which made the pores of the aerogel collapse to a certain extent. Combined with the data in Table 1, APT adhered to many tiny pores formed on OBC by GT, which increases the S_{BET} of imprinted aerogel and decreases the average pore size. The average pore size of I-APT-GT-OBC was 12.77 nm, and the S_{BET} was 28.01 $cm^2\ g^{-1}$. Significantly smaller than S_{BET} and pores of non-imprinted aerogels, which was believed to be due to the loss of APT in the material and a certain degree of fiber breakage in the BC caused by imprinting eluting and subsequent drying process. Imprinting eluting may also lead to pore collapse and pore volume reduction, resulting in pore size reduction. At the same time, due to the collapse of the hole, many particles may burn into one particle, and the specific surface area is relatively small. These results were consistent with SEM. Therefore, the introduction of APT could effectively increase the S_{BET} of the composite aerogel, which was beneficial to the subsequent adsorption of Dy(III), while the carboxylation and elution process would have a certain impact on the structural properties of the material.

Table 1 The pore structure parameters of four aerogels

Sample	Surface area ($cm^2\ g^{-1}$)	Pore size (nm)
BC	37.12	13.81
OBC	13.6	15.65
APT-GT-OBC	41.55	16.98
I-APT-GT-OBC	28.01	12.77

FT-IR

We analyzed the FT-IR spectra of the materials in the wave-number range of 4000 to 500 cm^{-1}, as shown in Fig. 4. It could be seen that the four aerogels all showed the characteristic peaks of BC at 3342 cm^{-1}, 2883 cm^{-1} and 1054 cm^{-1}, including -OH stretching vibration related to intramolecular and intermolecular hydrogen bonds, as well as stretching vibration of $–CH_2$ and C–O–C in cellulose glucose rings, respectively. Compared with the pure BC, the infrared

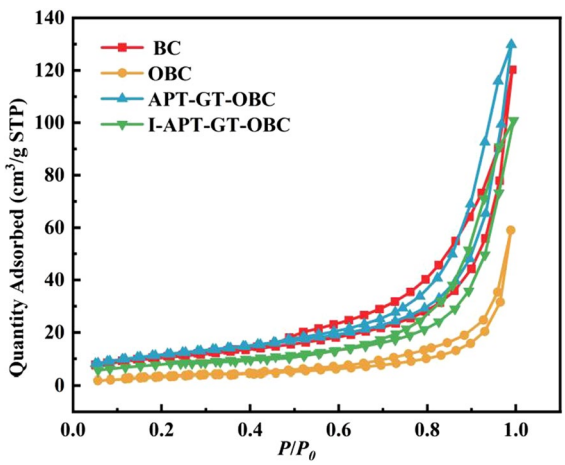

Fig. 3 N_2 adsorption–desorption isotherms of four aerogels

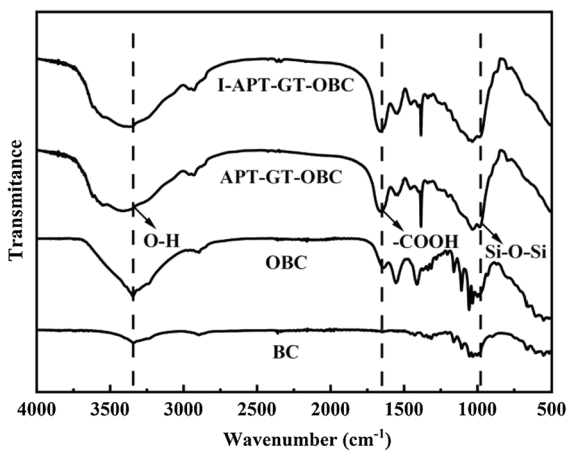

Fig. 4 FT-IR spectra of four aerogels

spectra of OBC, APT-GT-OBC and I-APT-GT-OBC all showed new a characteristic peak at 1654 cm^{-1}, this is mainly due to the anti-symmetrical stretching of –COOH in the carboxylate, indicating that TEMPO oxidation can convert hydroxyl groups on the surface of cellulose into carboxyl groups. Besides, the carboxyl characteristic peaks of the APT-GT-OBC and I-APT-GT-OBC aerogels were enhanced compared with OBC, which was due to the addition of GT. Against the spectrum of OBC, APT-GT-OBC and I-APT-GT-OBC appeared at 975 cm^{-1} with a new characteristic peak due to the presence of Si–O–Si (Song et al. 2020; Zhu et al. 2020) in APT. Therefore, it is concluded that TEMPO can effectively modify BC, APT and GT were successfully introduced into the composite aerogels.

TGA

Thermal stability tests were carried out on four aerogels under N_2. The mass loss of the aerogels at 30–800 °C was shown in Fig. 5. It could be seen that the mass loss of the four aerogels was relatively small below 200 °C, indicating that the residual water in the materials was very small. The BC and OBC had obvious mass loss at 200–350 °C, which decreased by about 80% and 55% respectively, which may be due to the thermal decomposition of the BC fiber structure. While APT-GT-OBC and I-APT-GT-OBC had only lost about 20% at this stage, which was due to the reduction of BC content in composites. The material entered the carbonization stage, and the loss of the material tended to stop after 450 °C. At this point the main component of BC and OBC residues is carbon, and the residual mass was 3.76% and 26.06%, respectively, while the main components of APT-GT-OBC and I-APT-GT-OBC residues were silicon and carbon. Therefore, the residual mass of these two kinds of composite aerogel were greatly improved compared with the former two. In other words, the carboxylation of BC and the addition of APT and GT can significantly enhance the thermal stability of the composite aerogel. The siloxane contained in ATP makes silicon and carbon still exist in the residue of composite aerogel at high temperature, which significantly reduces the mass loss of composite aerogels. Compared with APT-GT-OBC, I-APT-GT-OBC had a low total mass loss rate, which indicated that the thermal stability of the imprinted aerogel is better.

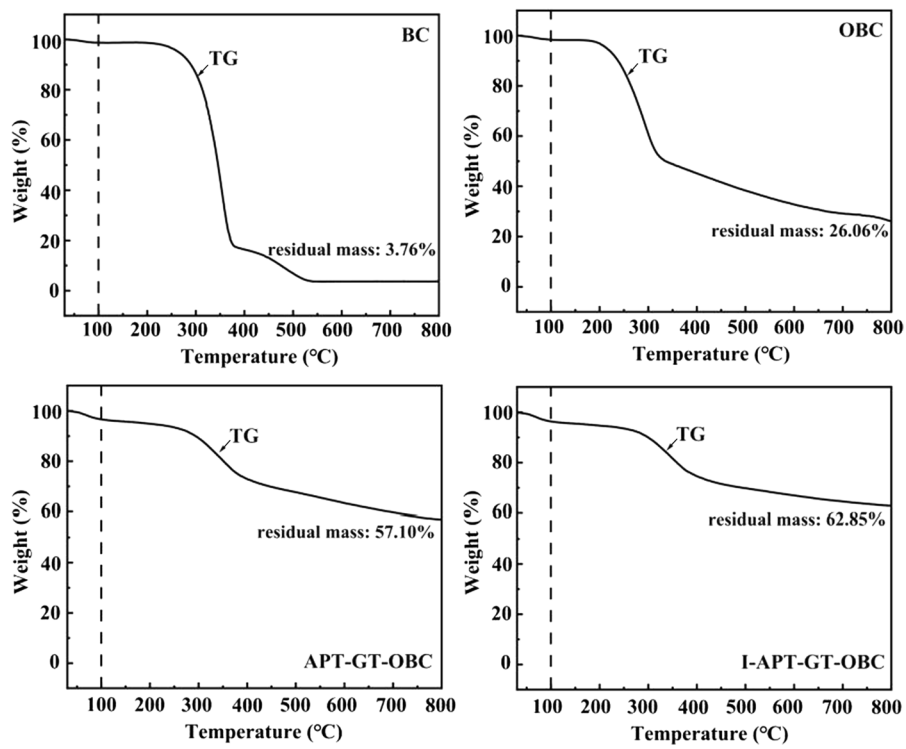

Fig. 5 TG curves of four aerogels

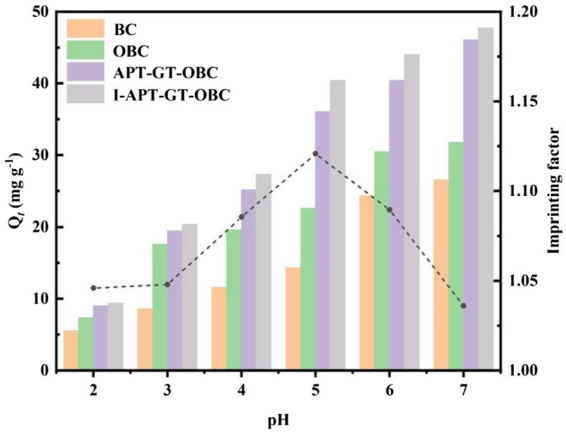

Fig. 6 Effect of pH on the adsorption properties of four aerogels

Analysis of adsorption results

Effect of pH on adsorption

We found the optimal adsorption pH by testing the adsorption capacity of four aerogels to Dy(III) at different pH values. Figure 6 showed the adsorption properties of these aerogels. It could be seen that the adsorption capacity of the pure BC, OBC, APT-GT-OBC and I-APT-GT-OBC aerogel for Dy(III) were gradually enhanced. Among them, the maximum adsorption amount of imprinted aerogel reached 47.74 mg g^{-1}. This demonstrated that carboxylation and the introduction of APT and GT further increased the active sites provided from the carboxyl groups, thus improving the ability of composite aerogel selection and adsorption of Dy(III). With the increase of pH value, the adsorption effect of aerogel changed significantly. The adsorption effect of all four aerogels increased slowly when the pH value was below 5.0. This is because the protonated carboxyl group will produce electrostatic repulsion with the Dy(III). The -COOH on aerogel surface inhibits the interaction between adsorbent and Dy(III). While when the pH value was 5.0, the adsorption capacity increased significantly. The protonation reaction of $–COO^{–}$ is weakened, and more active sites will coordinate with Dy(III) in the adsorbent, so the adsorption effect of aerogel is significantly improved. Especially for I-APT-GT-OBC, the adsorption capacity was significantly improved. Because of the imprinting process, the imprinted sites with specific structures enhanced the affinity of I-APT-GT-OBC for Dy(III). Therefore, at pH 5, the improvement of the adsorption capacity of I-APT-GT-OBC was greater than that of APT-GT-OBC. When the pH continued to rise, the –COOH on the surface of the aerogel continued to dissociate. At this time, the adsorption capacity of the imprinted material and the non-imprinted material still increased slowly. Which might be due to the increase rate of carboxyl dissociation decreased. The separation ability of the imprinted aerogel was measured by imprinting factor (IF). When the value of pH was 5.0, I-APT-GT-OBC showed a maximum IF value of 1.12. This showed that the imprinted aerogel has the best adsorption performance when pH = 5.0, so we set the pH to 5.0 in subsequent study of optimal conditions.

Adsorption dynamics

We tested the adsorption effects of four aerogels at different contact times and fitted them with PFOKM and PSOKM. Figure 7 and Table 2 were the adsorption data, the fitting curves and the related parameters, respectively. It is not difficult to see that the conclusion was the same as the pH adsorption experiment, the adsorption effect of APT-GT-OBC and I-APT-GT-OBC composite aerogel on Dy(III) was far superior to BC and OBC, which further reflected the necessity of subsequent material modification. In addition, the adsorption of the four aerogels occurred rapidly and began to reach

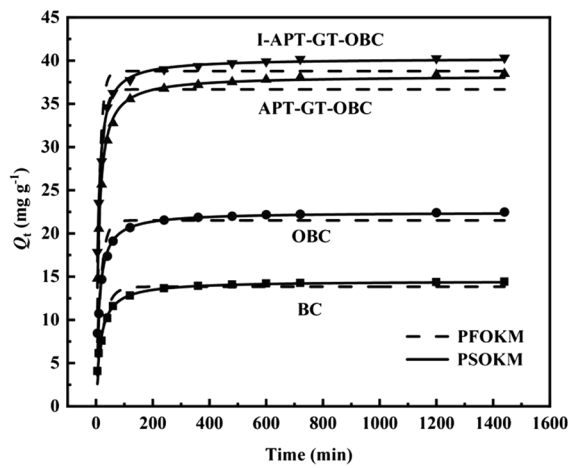

Fig. 7 Kinetic data and modeling for the adsorption of Dy(III)

Table 2 Kinetic parameters for fitting curves of PFOKM and PSOKM

Sorbents	PFOKM			PSOKM		
	Q_e (mg g^{-1})	k_1 (min^{-1})	R^2	Q_e (mg g^{-1})	k_2 (g mg^{-1} min^{-1})	R^2
BC	13.834	0.041	0.940	14.511	0.004	0.994
OBC	21.509	0.062	0.915	22.463	0.004	0.993
APT-GT-OBC	36.656	0.072	0.908	38.251	0.003	0.996
I-APT-GT-OBC	38.772	0.087	0.905	40.279	0.004	0.994

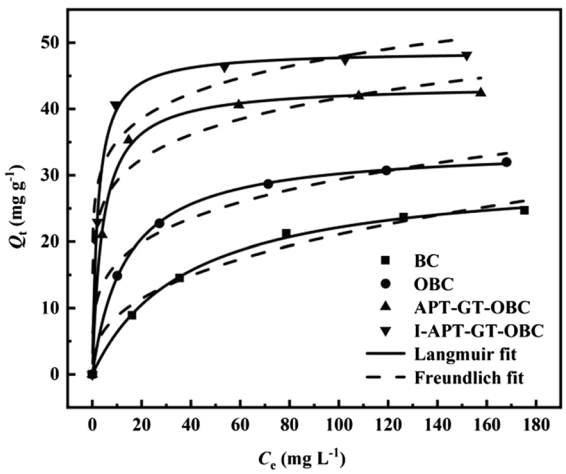

Fig. 8 Adsorption isotherm of Dy(III) by four aerogels

equilibrium in about 100 min, suggesting that BC itself was an excellent adsorbent for Dy(III). Combined with the fitting curves in the Fig. 7 and the correlation coefficient (R^2) in the table, compared with PFOKM, the fitting data of PSOKM is better, R^2 is 0.993 to 0.996, it could be seen that the fitting curves of the four aerogels were more consistent with PSOKM, which meant that the adsorption process of the prepared aerogels were mainly caused by chemical action, while physical action played an auxiliary role, and the adsorption occurs rapidly in a very short time.

Adsorption isotherm

We studied the influence of different initial concentrations on the adsorption effect of the aerogels, and obtained the maximum theoretical adsorption capacity and adsorption principle of aerogels by fitting adsorption data through Frundlich isothermal model and Langmuir isothermal model. The fitting curves and adsorption parameters were shown in Fig. 8 and Table 3, respectively. It could be seen that a higher initial concentration contributed to the adsorption of the aerogels. The closer the correlation parameter R^2 is to 1, the better the model fits. It could be seen that the isotherm data of the four aerogels and the Langmuir isotherm model had a better fitting effect, and the R^2 is 0.993–0.999, which meant that the adsorption for Dy(III) of the BC aerogel was mainly due to the monolecolar adsorption. In addition, through fitting analysis, it could be concluded that the maximum theoretical amount for Dy(III) of I-APT-GT-OBC was 48.762 mg g^{-1}, which was greatly improved compared with the OBC, pure BC and APT-GT-OBC aerogel.

Adsorption thermodynamics

We measured the ability of aerogels to adsorb Dy(III) at different temperatures to study the thermodynamic properties of these aerogels. Figure 9 showed the linear relationship between C_s and ln (Cs/C_e), and the

Table 3 Adsorption equilibrium constants for isotherm models

Sorbents	Langmuir			Freundlich		
	Q_m (mg g^{-1})	K_L (L mg^{-1})	R^2	K_F (mg g^{-1})	1/n	R^2
BC	30.597	0.026	0.995	3.648	0.381	0.932
OBC	34.298	0.074	0.999	9.587	0.243	0.933
APT-GT-OBC	43.650	0.246	0.993	20.388	0.155	0.805
I-APT-GT-OBC	48.762	0.455	0.994	25.778	0.134	0.773

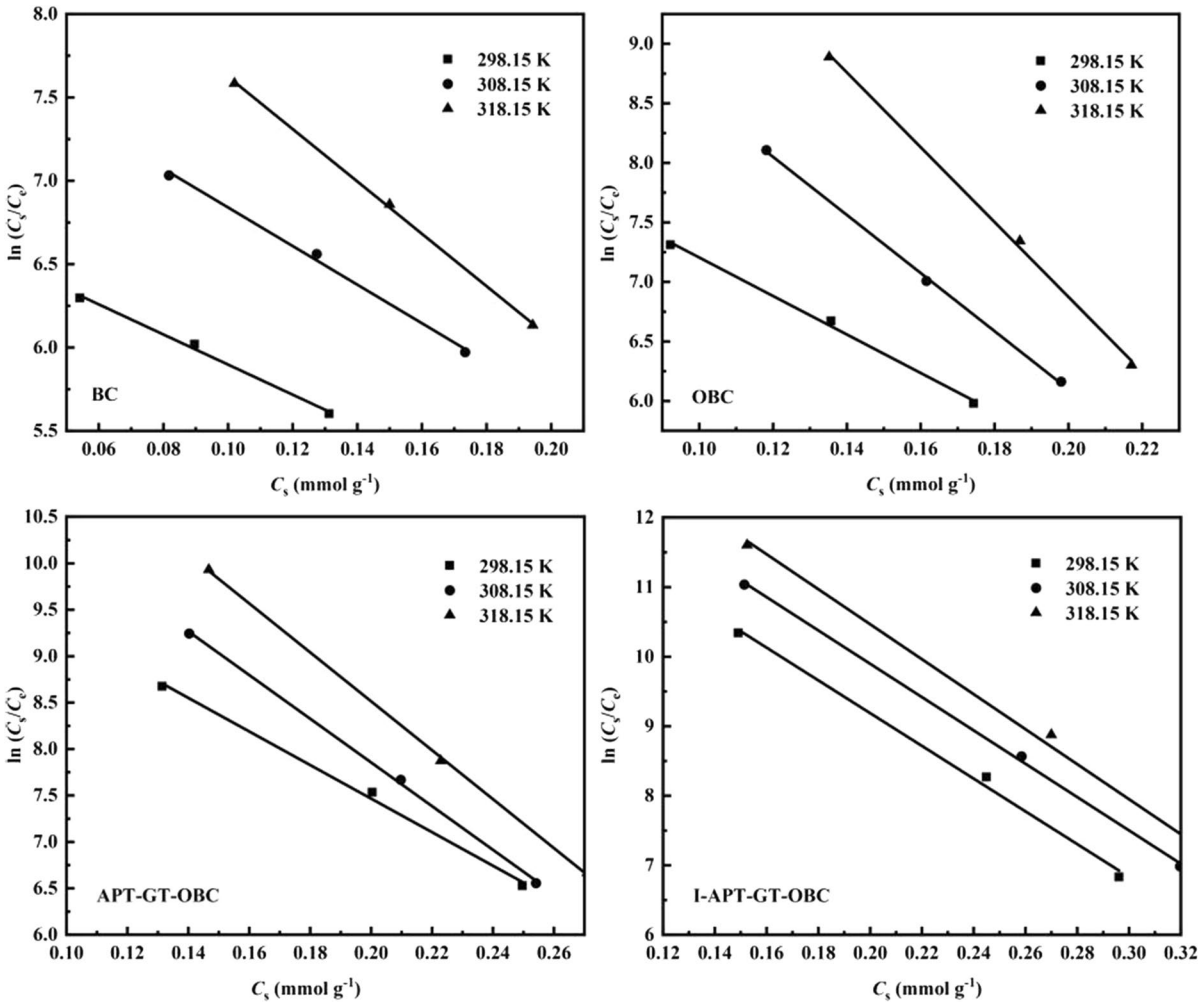

Fig. 9 Thermodynamic properties of aerogels at different temperatures: a plot of ln(C_s/C_e)

thermodynamic equilibrium constant K° is the vertical intercept value of the curve. Figure 10 showed the linear relationship between 1/T and the thermodynamic equilibrium constant K°. Table 4 showed the thermodynamic adsorption parameters such as ΔH°, ΔS° and ΔG°. The ΔH° value was less than zero, which meant that the adsorption process of Dy(III) by aerogel was an endothermic process, and a moderate increase in temperature could promote the occurrence of the reaction, mainly because the increase in temperature leaded to thermal diffusion of molecules, thus increasing the contact area of the adsorption reaction. The ΔS° value was greater than zero, which meant that the process of adsorption was a chaotic process. ΔG° values ranged from − 7.25 to − 4.75, all of which were less than zero, it is explained that the adsorption process of Dy(III) by aerogel was spontaneous. The value of ΔG° of the imprinted aerogel was the minimum, which meant that the adsorption of I-APT-GT-OBC aerogel was more spontaneous. In conclusion, the adsorption process of imprinted aerogels is an endothermic, entropy-enhancing and spontaneous process.

Selective test

To demonstrate the adsorption selectivity of the imprinted aerogel, we tested and compared the maximum adsorption effects of four aerogels when coexisting with Pr(III), Nd(III) and Dy(III) in a mixed

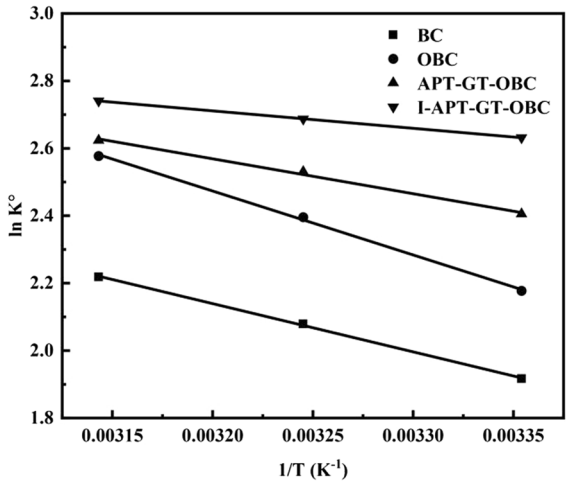

Fig. 10 Thermodynamic properties of four aerogels at different temperatures: lnK° degrees versus 1/T

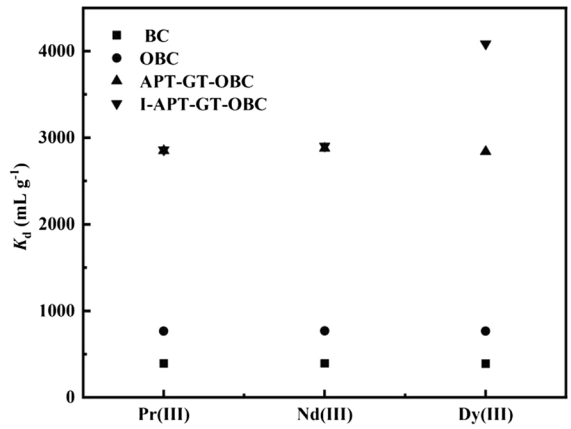

Fig. 11 The K_d values of different ions adsorbed by four aerogels

solution, and the separation constant (K_d) was used to analyze whether it is selective adsorption. The results were shown in Fig. 11 and Table 5. It could be seen that the ion imprinting technology played an advantage in competitive adsorption. Compared with Nd(III) and Pr(III), I-APT-GT-OBC had a higher separation constant for Dy(III), which was 4084.40 mL g^{-1}. In other words, the Dy(III) was the unique adsorption target for the I-APT-GT-OBC aerogel. There were pores in the imprinted aerogel that were specific for adsorption of Dy(III) and were unable to absorb other rare earth ions, which the other non-imprinted aerogels were unable to do. Through the competitive adsorption experiments, it was determined that I-APT-GT-OBC aerogel had a preference for Dy(III) during the adsorption process, and Dy(III) could be preferentially separated from multi-rare earth ionic solutions.

Repetitive experiment

In addition to the price of raw materials, the reusability of adsorbents also greatly affects the cost of the adsorption process. Recyclable adsorbents can greatly reduce the cost of separation and recovery, thus expanding the application range of adsorbents. As shown in Fig. 12, in order to verify the reusability of I-APT-GT-OBC aerogels, five adsorption–desorption experiments were performed on the aerogels, and the adsorption capacity of each cycle was tested

Table 4 Thermodynamic parameters of four aerogels

Sorbents	ΔH° (kJ mol^{-1})	ΔS° (J mol^{-1})	T (K)	K°	ΔG° (kJ mol^{-1})	R^2
BC	4.30	36.33	298.15	6.80	− 4.75	0.999
			308.15	8.00	− 5.33	
			318.15	9.19	− 5.87	
OBC	8.61	48.89	298.15	8.82	− 5.40	0.998
			308.15	10.98	− 6.14	
			318.15	13.16	− 6.82	
APT-GT-OBC	15.77	71.00	298.15	11.08	− 5.96	0.991
			308.15	12.56	− 6.48	
			318.15	13.78	− 6.94	
I-APT-GT-OBC	11.90	55.87	298.15	13.90	− 6.52	0.999
			308.15	14.69	− 6.88	
			318.15	15.50	− 7.25	

Table 5 The K_d value of Dy(III) adsorbed by four aerogels in mixed solution

Cation	BC		OBC		APT-GT-OBC		I-APT-GT-OBC	
	C_f (mg L^{-1})	K_d (mL g^{-1})	C_f (mg L^{-1})	K_d (mL g^{-1})	C_f (mg L^{-1})	K_d (mL g^{-1})	C_f (mg L^{-1})	K_d (mL g^{-1})
Pr(III)	35.911	392.33	28.292	767.28	12.993	2848.23	12.958	2858.62
Nd(III)	35.873	393.81	28.253	769.72	12.898	2876.57	12.81	2903.20
Dy(III)	35.977	389.78	28.314	765.91	13.027	2838.18	9.834	4084.40

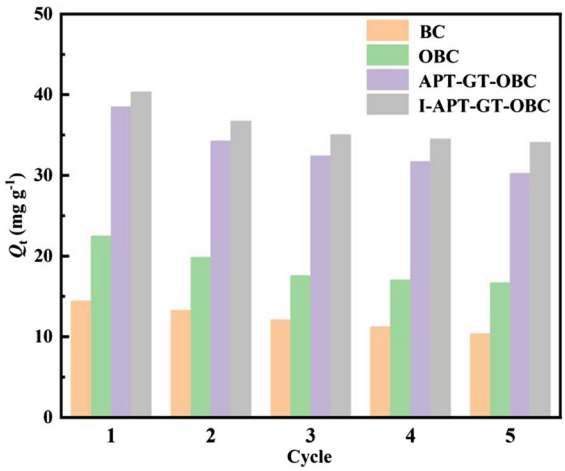

Fig. 12 Regeneration of four aerogels

respectively. It could be seen that the adsorption capacities after five cycles of the pure BC, OBC, APT-GT-OBC and I-APT-GT-OBC were 71.9%, 74.3%, 78.5% and 84.5% of the first adsorption, respectively. The decrease of adsorption capacities was mainly due to the destruction of pore structure during the elution (SEM images of I-APT-GT-OBC after five cycles are shown in support materials), but all showed good stability. In other words, compared with non-imprinted aerogel, the imprinted aerogel showed stronger stability and reusability after multiple adsorption cycles.

Conclusions

In this paper, a low-cost and reusable I-APT-GT-OBC aerogel was prepared by the ion-imprinting technology with BC as the basic structure, and two kinds of cheap raw materials such as APT and GT were introduced to maintain the efficient adsorption for Dy(III) of aerogels while reducing adsorbent cost. A series of characterization methods showed that the I-APT-GT-OBC aerogel was successfully synthesized, and the imprinted aerogel possessed many tiny pores for the adsorption of Dy(III). The theoretical maximum adsorption capacity of I-APT-GT-OBC aerogel on Dy(III) was 48.762 mg g^{-1}, and the adsorption process was mainly controlled by chemical adsorption. Competitive ions adsorption experiments and reusable experiments showed that I-APT-GT-OBC aerogel had good selectivity and stability to Dy(III).

Author contributions All authors contributed to the study conception and design. Material preparation, data collection and analysis were performed by XZ, TX, WS, JM, MZ and ZL. The first draft of the manuscript was written by WS and all authors commented on previous versions of the manuscript. All authors read and approved the final manuscript.

Funding The authors are supported by the National Natural Science Foundation of China (Grant Nos. 21876015, 21878026, 22008014). In addition, the author also appreciates the technical support provided by the Analysis and Test Center of Changzhou University in SEM, TGA and FTIR.

Declarations

Competing interests The authors declare that they have no known competing financial interests or personal relationships that could have appeared to influence the work reported in this paper.

References

Alguacil FJ, Garcia-Diaz I, Baquero EE, Largo OR, Lopez FA (2020) On the adsorption of cerium(III) using multiwalled carbon nanotubes. Metals. https://doi.org/10.3390/met10081057

Ashour RM, Abdelhamid HN, Abdel-Magied AF, Abdel-Khalek AA, Ali MM, Uheida A, Muhammed M, Zou XD, Dutta J (2017) Rare earth ions adsorption onto graphene oxide nanosheets. Solvent Extr Ion Exch 35(2):91–103. https://doi.org/10.1080/07366299.2017.1287509

Briao GV, Carlos da Silva MG, Adeodato Vieira MG (2021) Dysprosium adsorption on expanded vermiculite: kinetics, selectivity and desorption. Colloid Surf A. https://doi.org/10.1016/j.colsurfa.2021.127616

Devi AP, Mishra PM (2019) Biosorption of dysprosium (III) using raw and surface-modified bark powder of *Mangifera indica*: isotherm, kinetic and thermodynamic studies. Environ Sci Pollut Res 26(7):6545–6556. https://doi.org/10.1007/s11356-018-04098-7

Doineau E, Bauer G, Ensenlaz L, Novales B, Sillard C, Benezet J-C, Bras J, Cathala B, Moigne NL (2020) Adsorption of xyloglucan and cellulose nanocrystals on natural fibres for the creation of hierarchically structured fibres. Carbohydr Polym. https://doi.org/10.1016/j.carbpol.2020.116713

Fu J, Chen L, Li J, Zhang Z (2015) Current status and challenges of ion imprinting. J Mater Chem A 3(26):13598–13627. https://doi.org/10.1039/c5ta02421h

Hoshina H, Chen JH, Amada H, Seko N (2020) Chain entanglement of 2-ethylhexyl hydrogen-2-ethylhexylphosphonate into methacrylate-grafted nonwoven fabrics for applications in separation and recovery of Dy (III) and Nd (III) from aqueous solution. Polymers. https://doi.org/10.3390/polym12112656

Hu X, Yan L, Wang Y, Xu M (2021) Ice segregation induced self-assembly of salecan and grapheme oxide nanosheets into ion-imprinted aerogel with superior selectivity for cadmium (II) capture. Chem Eng J. https://doi.org/10.1016/j.cej.2020.128106

Kaneko T, Nagata F, Kugimiya S, Kato K (2018) Optimization of carboxyl-functionalized mesoporous silica for the selective adsorption of dysprosium. J Environ Chem Eng 6(5):5990–5998. https://doi.org/10.1016/j.jece.2018.09.018

Kedzior SA, Gabriel VA, Dube MA, Cranston ED (2021) Nanocellulose in emulsions and heterogeneous water-based polymer systems: a review. Adv Mater. https://doi.org/10.1002/adma.202002404

Li ML, Ji ZH, Sheng GD, Zhou SD, Chang KK, Jin EQ, Guo XJ (2021) Scavenging mechanism of rare earth metal ions in water by graphene oxide. J Mol Liq. https://doi.org/10.1016/j.molliq.2020.114940

Liao Y, Wang M, Chen DJ (2018) Production of three-dimensional porous polydopamine-functionalized attapulgite/chitosan aerogel for uranium(VI) adsorption. J Radioanal Nucl Chem 316(2):635–647. https://doi.org/10.1007/s10967-018-5816-2

Lin JB, Gu Y, Sun BJ, Li WP, Qu X, Sun DP (2021) A one-pot biosynthesis of an aerogel composite based on attapulgite clay/bacterial cellulose to remove Pb^{2+} ion. Micro Nano Lett 16(8):405–412. https://doi.org/10.1049/mna2.12033

Long LY, Weng YX, Wang YZ (2018) Cellulose aerogels: synthesis, applications, and prospects. Polymers. https://doi.org/10.3390/polym10060623

Marciano JS, Ferreira RR, de Souza AG, Barbosa RFS, de Moura AJ, Rosa DS (2021) Biodegradable gelatin composite hydrogels filled with cellulose for chromium (VI) adsorption from contaminated water. Int J Biol Macromol 181:112–124. https://doi.org/10.1016/j.ijbiomac.2021.03.117

Monier M, Abdel-Latif DA (2013) Synthesis and characterization of ion-imprinted chelating fibers based on PET for selective removal of Hg^{2+}. Chem Eng J 221:452–460. https://doi.org/10.1016/j.cej.2013.02.003

Moradi E, Mehrani Z, Ebrahimzadeh H (2020) Gelatin/sodium triphosphate hydrogel electrospun nanofiber mat as a novel nanosorbent for microextraction in packed syringe of La^{3+} and Tb^{3+} ions prior to their determination by ICP-OES. React Funct Polym. https://doi.org/10.1016/j.reactfunctpolym.2020.104627

Oshima T, Kondo K, Ohto K, Inoue K, Baba Y (2008) Preparation of phosphorylated bacterial cellulose as an adsorbent for metal ions. React Funct Polym 68(1):376–383. https://doi.org/10.1016/j.reactfunctpolym.2007.07.046

Padhan E, Nayak AK, Sarangi K (2017) Recovery of neodymium and dysprosium from NdFeB magnet swarf. Hydrometallurgy 174:210–215. https://doi.org/10.1016/j.hydromet.2017.10.015

Pegier M, Kilian K, Pyrzynska K (2019) Kinetics of scandium ion sorption onto oxidized carbon nanotubes. Monatsh Chem 150(9):1569–1572. https://doi.org/10.1007/s00706-019-02472-w

Sakwises L, Rodthongkum N, Ummartyotin S (2017) SnO2- and bacterial-cellulose nanofiber-based composites as a novel platform for nickel-ion detection. J Mol Liq 248:246–252. https://doi.org/10.1016/j.molliq.2017.10.047

Salimian S, Zadhoush A, Naeimirad M, Kotek R, Ramakrishna S (2018) A review on aerogel: 3D nanoporous structured fillers in polymer-based nanocomposites. Polym Compos 39(10):3383–3408. https://doi.org/10.1002/pc.24412

Shang SS, Ye X, Jiang X, You Q, Zhong Y, Wu XD, Cui S (2021) Preparation and characterization of cellulose/attapulgite composite aerogels with high strength and hydrophobicity. J Non-Cryst Solids. https://doi.org/10.1016/j.jnoncrysol.2021.120922

Song S, Liu Z, Zhang J, Jiao C, Ding L, Yang S (2020) Synthesis and adsorption properties of novel bacterial cellulose/graphene oxide/attapulgite materials for Cu and Pb ions in aqueous solutions. Materials (basel). https://doi.org/10.3390/ma13173703

Xu XR, Chen X, Yang LY, Zhao YX, Zhang X, Shen RQ, Sun DP, Qian JS (2020) Film-like bacterial cellulose based molecularly imprinted materials for highly efficient recognition and adsorption of cresol isomers. Chem Eng J. https://doi.org/10.1016/j.cej.2019.123007

Yadav KK, Anitha M, Singh DK, Kain V (2018) NdFeB magnet recycling: dysprosium recovery by non-dispersive solvent extraction employing hollow fibre membrane contactor. Sep Purif Technol 194:265–271. https://doi.org/10.1016/j.seppur.2017.11.025

Yan ZF, Zhu KX, Li XQ, Wu X (2022) Recyclable bacterial cellulose aerogel for oil and water separation. J Polym Environ. https://doi.org/10.1007/s10924-021-02369-y

Zhang YZ, Bian TT, Jiang R, Zhang Y, Zheng XD, Li ZY (2021) Bionic chitosan-carbon imprinted aerogel for high selective recovery of Gd(III) from end-of-life rare earth productions. J Hazard Mater. https://doi.org/10.1016/j.jhazmat.2020.124347

Zheng X, Zhang Y, Bian T, Wang D, Li Z (2019) One-step fabrication of imprinted mesoporous cellulose nanocrystals films for selective separation and recovery of Nd(III). Cellulose 26(9):5571–5582. https://doi.org/10.1007/s10570-019-02482-1

Zheng X, Sun W, Li A, Wang B, Jiang R, Song Z, Zhang Y, Li Z (2022a) Graphene oxide and polyethyleneimine cooperative construct ionic imprinted cellulose nanocrystal aerogel for selective adsorption of Dy(III). Cellulose 29(1):469–481. https://doi.org/10.1007/s10570-021-04299-3

Zheng X, Sun W, Li A, Zhang Y, Li Z (2022b) Bacterial cellulose nanofibrous ion imprinted aerogel for highly efficient recognition and adsorption of Dy(III). Process Saf Environ 160:70–79. https://doi.org/10.1016/j.psep.2022b.01.077

Zhu J, Zhao F, Xiong R, Peng T, Ma Y, Hu J, Xie L, Jiang C (2020) Thermal insulation and flame retardancy of attapulgite reinforced gelatin-based composite aerogel with enhanced strength properties. Compos Part A-Appl S. https://doi.org/10.1016/j.compositesa.2020.106040